arXiv:1604.00489v2 [cond-mat.stat-mech] 26 Jul 2016

Occurrence of discontinuities in the performance of finite-time quantum Otto cycles

Yuanjian Zheng,[1,2] Peter Hänggi,[3,4,5] and Dario Poletti[1,6]

[1] *Engineering Product Development Pillar, Singapore University of Technology and Design, 8 Somapah Road, 487372 Singapore*
[2] *Division of Physics and Applied Physics, School of Physical and Mathematical Sciences, Nanyang Technological University, 21 Nanyang Link, 637371 Singapore*
[3] *Institut für Physik, Universität Augsburg, Universitätsstraße 1, D-86135 Augsburg, Germany*
[4] *Nanosystems Initiative Munich, Schellingstr. 4, D-80799 München, Germany*
[5] *Department of Physics, National University of Singapore, 117542 Singapore, Republic of Singapore*
[6] *MajuLab, CNRS-UNS-NUS-NTU International Joint Research Unit, UMI 3654, Singapore*

We study a quantum Otto cycle in which the strokes are performed in finite time. The cycle involves energy measurements at the end of each stroke to allow for the respective determination of work. We then optimize for the work and efficiency of the cycle by varying the time spent in the different strokes and find that the optimal value of the ratio of time spent on each stroke goes through sudden changes as the parameters of this cycle vary continuously. The position of these discontinuities depends on the optimized quantity under consideration such as the net work output or the efficiency.

I. INTRODUCTION

Recent years have witnessed a rapid growth in the study of heat engines operating at the nanoscale. More generally, this area of research is increasingly progressing towards a multitude of energy efficient nano-technologies [1–5]. On the experimental front, there have been several realizations of mesoscopic heat engines that employ a wide range of working fluids, albeit operating almost exclusively in the classical domain. Typical examples include piezoelectric materials [6], colloidal systems [7] and even a single atom [8], to name but a few.

On the other hand, our theoretical understanding of quantum thermodynamics has undergone considerable development that has enhanced our ability to manipulate and control thermal devices at the nanoscale. For example, with the use of tailored driving protocols in various strategies collectively termed shortcuts to adiabaticity, we are equipped to generate adiabatic or adiabatic-like dynamics in systems that are driven within a finite amount of time [9–21]. However their practical usefulness is conditional upon the relative timescales of the cycle and the nature of the driving fields [22]. More recently, studies of many-body working fluids in thermodynamic cycles are providing guiding principles that can enhance the performance of quantum heat engines. For instance, quantum statistics has been shown to significantly influence the work distribution of Hamiltonian processes [23, 24]. In particular, the interplay between quantum statistics and other properties of the working fluid such as the trap geometry [25] and/or many-body interactions [26] can result in augmenting the performance of a heat engine operating in the quantum regime. See [4, 27–30] for recent reviews on quantum thermodynamics and heat engines.

Furthermore, our understanding of heat engines at the nanoscale has benefited from salient advances in statistical physics, namely the area of fluctuation theorems [31–35]. Among the various fundamental relations, we mention in particular the Jarzynski equality that has been validated experimentally in the classical regime, e.g. see Refs. [31, 32, 36]. Although presenting a formidable challenge for experiment, the Jarzynski equality has also been verified also in the quantum regime [37, 38]. These fluctuation relations allow us to explore various peculiarities in the thermodynamic behavior of non-equilibrium heat engines [39, 40]. Such peculiarities may arise from (but are not limited to) squeezed or non-thermal baths [41–45], irreversibility [46, 47], finite-time effects of the driving [48, 49], and more recently from the time-asymmetry used in the driving protocol [50, 51]. Moreover, cycles that contain sudden changes in the Hamiltonian parameters have also been investigated [52–55], thereby accounting for the role of noise in the cycles' performance as well [56, 57].

In this study, we further develop the understanding of non-equilibrium heat engines that operate during an overall time span τ upon employing strokes that are individually performed in finite time. In our analysis of the cycle, we introduce an explicit projective energy measurement which is performed before and after each stroke of the cycle, so as to determine the work via the two-time energy measurements protocol [58]. We then explore the non-equilibrium behavior by exploring the conditions for optimal work output and efficiency of the cycle and find characteristic discontinuities as a function of the system parameters.

In section (II) we describe the Otto cycle setup and detail the relevant parameters and figure of merits of the quantum engine. The Otto cycle is composed of four strokes: two unitary strokes, of total time τ_u, intercalated by two strokes in which the system is weakly coupled to baths, for a total time τ_b. Hence the total duration of the cycle is $\tau = \tau_u + \tau_b$. We consider a single ion in a harmonic trap as the the working substance of the system, while each bath consists of two lasers weakly coupled to the system, which raise and lower the occupation number of the quantum harmonic oscillator at different rates. The overall effect of this weak system-bath interaction is such that after sufficient time has elapsed, the system

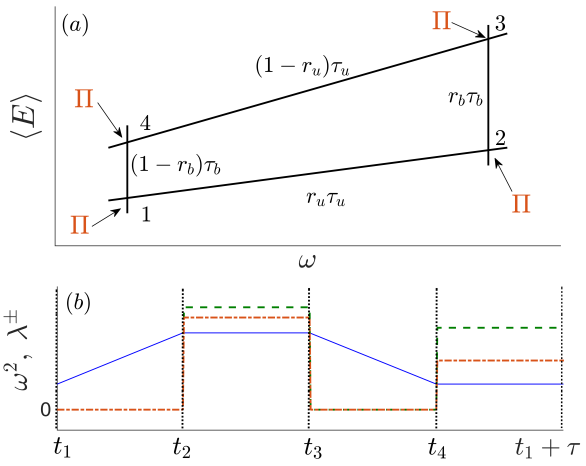

FIG. 1. (color online) (a) **Schematics of a quantum Otto Cycle of total time duration $\tau = \tau_u + \tau_b$.** Mean energy $\langle E \rangle$ versus a time-dependent manipulation of the trap frequency $\omega(t)$: $1 \to 2$. Compression: Unitary (subscript u) time evolution using a linearly increasing $\omega^2(t)$ during the time span $r_u\tau_u$. $2 \to 3$: Iso-parametric coupling to the hot bath (subscript b) at effective temperature $1/\beta_3$ during time $r_b\tau_b$. $3 \to 4$: Expansion: Unitary time evolution with linearly decreasing $\omega^2(t)$ during time interval $(1-r_u)\tau_u$. $4 \to 1$: Iso-parametric coupling to the cold bath at effective temperature $1/\beta_1$ in remaining time span $(1-r_b)\tau_b$. Projective energy measurements $\Pi\left(\hat{\rho}(t_i)\right)$ are executed at the end of each stroke. (b) **Time Dependence of Cycle Parameters.** The square of the angular frequency variation $\omega^2(t)$, depicted by the blue continuous line, increases linearly between t_1 and $t_2 = t_1 + r_u\tau_u$ while the bath coupling parameters $\lambda^{\pm}$, given by the red dot-dashed line (λ^+) and the green dashed line (λ^-), respectively, are held at vanishing values (zero system-bath coupling). Subsequently, after an instantaneous energy measurement and until time $t_3 = t_2 + r_b\tau_b$, both $\lambda^{\pm}$ are abruptly adjusted to values which yield the hot effective temperature, $1/\beta_3$, while $\omega^2(t)$ is held fixed. After yet another energy measurement and till time $t_4 = t_3 + (1-r_u)\tau_u$, the angular frequency $\omega^2(t)$ is linearly reduced while the bath-coupling strengths $\lambda^{\pm}$ are again switched to zero. In the last stroke between t_4 and $t_1 + \tau$ the angular frequency is held fixed while the $\lambda^{\pm}$ are turned to their new respective values corresponding to a lower effective temperature, $1/\beta_1$. Projective energy measurements are represented by vertical black dotted lines. Note that the ratio λ^+/λ^- is different in the strokes indicating different effective temperatures in the two baths.

becomes a thermal-like state at an effective temperature determined by a ratio involving the raising and lowering occupation number rates.

In section (III) we first analyze the limiting case of the ideal bath couplings where the system relaxes to final states that are effectively thermal-like at the end of the two dissipative strokes.

In the following section (IV) we generalize our study to the case of an engine cycle in which the dissipative strokes are not coupled for long enough times to bring the system to a thermal-like state. Lastly, we summarize our main findings and present our conclusions in section (V).

II. MODEL

We study as an idealized model for a quantum Otto cycle a one dimensional harmonic oscillator whose trapping frequency can be controlled in time and which is *weakly* coupled to external baths [61], see Fig. (1). We focus on a particular experimental realization made with a single ion in a Paul trap which can be cooled and heated via side-band cooling by the use of two simultaneously acting lasers [62]. The evolution of the density operator $\hat{\rho}(t)$ of the system to the external baths can thus be described by a master equation in (Markovian) Lindblad form [63, 64],

$$\frac{d\hat{\rho}}{dt} = -\frac{\mathrm{i}}{\hbar}\left[\hat{H}(t), \hat{\rho}\right] + \mathcal{D}(\hat{\rho}, t)\ . \tag{1}$$

The time-dependent system Hamiltonian is explicitly given by

$$\hat{H}(t) = \left(\hat{n} + \frac{1}{2}\right)\hbar\omega(t) \tag{2}$$

Here, $\hat{n} = \hat{a}^\dagger\hat{a}$ is the number operator and $\hat{a}$ ($\hat{a}^\dagger$) is the lowering (raising) operator, while $\omega(t)$ denotes the time-dependent frequency of the trap. The dissipator $\mathcal{D}(\rho, t)$ in (1) is given by [65]:

$$\begin{aligned}\mathcal{D}(\hat{\rho}, t) = \lambda^+(t)\left(2\hat{a}^\dagger\hat{\rho}\hat{a} - \left\{\hat{a}\hat{a}^\dagger, \hat{\rho}\right\}\right) \\ + \lambda^-(t)\left(2\hat{a}\hat{\rho}\hat{a}^\dagger - \left\{\hat{a}^\dagger\hat{a}, \hat{\rho}\right\}\right)\ ,\end{aligned} \tag{3}$$

where λ^+ and λ^- denote the raising and lowering occupation rates respectively. Note that as a consequence of the protocol used for $\omega^2(t)$ (see Fig. 1), the system Hamiltonian does not change in time during the dissipative parts of the cycle when the external baths are acting on the system. Given a fixed trapping frequency ω, the dissipator tends to drive the system towards the diagonal quantum state that assumes the form

$$\hat{\rho} = \sum_n \rho_{nn}|n\rangle\langle n| = \sum_n \frac{e^{-(n+1/2)\beta\hbar\omega}}{Z(\beta,\omega)}|n\rangle\langle n|\ , \tag{4}$$

where ρ_{nn} denotes the normalized occupation probability in state $|n\rangle$, being the eigenstate of the Hamiltonian (2) and the effective inverse temperature β of the steady state is such that $\lambda^+/\lambda^- = e^{-\beta\hbar\omega}$. $Z(\beta,\omega)$ is the partition function of a 1D harmonic oscillator at inverse temperature β and trapping frequency ω, and is given by

$$Z(\beta,\omega) = \frac{e^{-\beta\hbar\omega/2}}{1 - e^{-\beta\hbar\omega}}. \tag{5}$$

The relative strengths of λ^+ and λ^- determine the effective temperature for the system, provided that the

steady state is reached. We would like to emphasize that although the baths considered can prepare a single ion in a thermal-like state, they do not constitute actual thermal baths. Instead, they impose a certain distribution of occupation of the energy levels that is independent of the energy difference between the levels. Given the non-thermal property of the baths we prefer to refer more precisely to the specific steady state of the (time independent) master equation as 'thermal-like' and to β as an 'effective' inverse temperature.

Next we consider the operation of the quanutm Otto engine in greater detail, see Fig. 1. The cycle consists of two *unitary* strokes, each followed by a corresponding dissipative stroke in which the system is weakly coupled to the environment while the system parameters are held fixed (iso-parametric processes) [25, 60]. We stress that the dissipative coupling is based on the weak coupling assumption, where the raising and lowering rates are much smaller than the internal electronic levels of the ion. In complete analogy to the classical Otto cycle, no heat is thus being exchanged during the unitary strokes $1 \to 2$ and $3 \to 4$, while no work is done during the iso-parametric processes $2 \to 3$ and from $4 \to 1$ of the cycle (see below for a more detailed explanation).

The evaluation of quantum work fluctuations [58, 66, 67] requires nonselective, projective energy measurements on the *total* combined system composed of the system, the baths and the mutual system-bath interactions [67, 68]. The determination of work in a stroke operation thus mandates (nonselective) energy measurements to be applied before and after each stroke of the Otto cycle.

Typically this presents a formidable challenge, both for theory and even more so for experiments. This difficult task persists *even* in the case in which the coupling among the baths and the system of interest is weak [69]. Namely, with all energetic contributions of the system-bath interactions being neglected, the work fluctuations for the system are still composed of both the changes in the internal energy of the system and, in general, finite energy exchanges with the baths.

Both these contributions are typically non-vanishing. However, the difficult task becomes feasible if for instance, the average heat exchange is vanishing, yielding an average work exchange $\langle W\rangle$ that is equal to the change of the energy of the system $\langle \Delta E\rangle$, i.e. $\langle W\rangle = \langle \Delta E\rangle$ [70]. Likewise, when the work on the total system is vanishing, it implies that the change of the energy of the system alone is determined solely by the typically quite intricate heat exchange Q among the baths and the system, i.e. $\langle \Delta E\rangle = \langle Q\rangle$. In this case the projective measurement of the (nonselective) bare system energy alone is sufficient [70]. It thus demands that the quantum state given by the corresponding reduced density operator must be calculated. This in turn allows the overall average exchanges of either work or heat to be evaluated.

We next introduce a nonselective energy postmeasurement following each stroke of the cycle. This can be formalized by writing down the corresponding (postmeasurement) density operators explicitly. The average energies are obtained in terms of projective energy measurements of the corresponding quantum state of the Otto engine. By introducing the projection operator $\Pi_n(t) = |n(t)\rangle\langle n(t)|$, where $|n(t)\rangle$ is the instantaneous n-th energy eigenstate of the corresponding time-frozen system Hamiltonian at time t, the effect of the postmeasurement on the state at time t is then given by a nonselective quantum state, and the reduced density operator $\hat{\rho}(t^+)$ that reads

$$\hat{\rho}(t^+) = M_t\big(\hat{\rho}(t)\big) = \sum_n \Pi_n(t)\hat{\rho}(t)\Pi_n(t)\ . \tag{6}$$

Since we are primarily interested in studying time-asymmetric protocols, we consider cycles in which a total time span τ_u is spent on the unitary strokes and a total time τ_b on the dissipative strokes. We further parametrize the distribution of the time intervals within the unitary and dissipative strokes to allow for asymmetry in the driving protocol. For instance the time spent on the compression stroke $1 \to 2$, is given by $t_2 - t_1 = r_u\tau_u$ where r_u is a real number between 0 and 1, while the time spent on the expansion stroke, $3 \to 4$, is given by $t_4 - t_3 = (1-r_u)\tau_u$. Similarly, for the dissipative strokes, coupling to the hot bath $2 \to 3$ is performed in time $t_3 - t_2 = r_b\tau_b$ and to the cold bath $4 \to 1$, in time $t_1 + \tau - t_4 = (1 - r_b)\tau_b$.

For the unitary strokes of the cycle, we consider a protocol in which $\omega^2(t)$ varies linearly between ω_1 and ω_2, such that $\omega^2(t) = \omega_1^2 + (\omega_2^2 - \omega_1^2)(t-t_1)/r_u\tau_u$ for the compression stroke and $\omega^2(t) = \omega_2^2 + (\omega_1^2 - \omega_2^2)(t - t_3)/[(1 - r_u)\tau_u]$ for the expansion stroke. Here we have used t_1 and t_3 respectively for the times at which the system is at stages 1 and 3 of the cycle. A plot of the time dependence of $\omega^2(t)$ is given in Fig. 1(b) (continuous blue line).

On the dissipative end of things, the coupling to the hot bath is turned on instantaneously at time t_2^+ from zero to the values $\lambda_3^\pm$ and back to zero at time t_3. Similarly, on the cold end, the bath couplings are again instantaneously switched from zero to $\lambda_1^\pm$ for the time between t_4^+ and $t_1 + \tau$. A depiction of the change of $\lambda^\pm$ is given in Fig. 1(b), where the green-dashed line represents λ^- and the dot-dashed red line depicts λ^+. Note that $\lambda^- > \lambda^+$ and that their ratio is different in the two dissipative strokes, indicating that the system is driven towards different Gibbs-like states.

In the following we use the notation $S_{a\to b}(\hat{\rho})$ for the map corresponding to the stroke from a to b acting on the state $\hat{\rho}$. Explicitly, considering a postmeasurement density operator $\hat{\rho}(t_1^+)$ for the system, just after an energy measurement, the various strokes are given by

$$\begin{aligned}\hat{\rho}(t_2^+) &= S_{1\to 2}\left(\hat{\rho}(t_1^+)\right)\\ &= M_{t_2}\Big(K_{t_1,t_2}\hat{\rho}(t_1^+)\Big)\end{aligned} \tag{7}$$

where $K_{t,t'}(\hat{\rho}(t)) = \hat{U}_{t,t'}\hat{\rho}(t)\hat{U}^{\dagger}_{t,t'}$ with $\hat{U}_{t,t'} = \mathcal{T}\exp\left(-\mathrm{i}\int_t^{t'}\hat{H}(s)ds\right)$ and $\mathcal{T}$ denotes time ordering. It then follows that

$$\begin{aligned}\hat{\rho}(t_3^+) &= S_{2\to3}\left(\hat{\rho}(t_2^+)\right)\\ &= M_{t_3}(\Lambda_{t_2,t_3,\omega_2,\lambda_3^{\pm}}\hat{\rho}(t_2^+))\end{aligned} \tag{8}$$

where $\Lambda_{t_2,t_3,\omega_2,\lambda_3^{\pm}}$ is a non-unitary map that evolves a density operator $\hat{\rho}(t)$ from t_2^+ to t_3 using the dissipative Lindblad master equation (1-3) with $\omega(t)=\omega_2$ and $\lambda^{\pm}(t)=\lambda_3^{\pm}$, where the parameters are time independent. The cycle closes upon applying the last two strokes; i.e.,

$$\begin{aligned}\hat{\rho}(t_4^+) &= S_{3\to4}\left(\hat{\rho}(t_3^+)\right)\\ &= M_{t_4}(K_{t_3,t_4}\hat{\rho}(t_3^+))\end{aligned} \tag{9}$$

and back to the initial steady state, a fixed point of the cycle composed of four strokes, i.e.,

$$\begin{aligned}\hat{\rho}(t_1^+ + \tau) = \hat{\rho}(t_1^+) &= S_{4\to1}\left(\hat{\rho}(t_4^+)\right)\\ &= M_{t_1}(\Lambda_{t_4,t_1+\tau,\omega_1,\lambda_1^{\pm}}\hat{\rho}(t_4^+))\end{aligned} \tag{10}$$

The steady state of the map is thus used to characterize the cycle given by the combination of the four strokes, which in our case is unique, and is equivalent to the diagonal fixed point, obeying

$$\hat{\rho}(t_1^+) = S_{4\to1}\Big(S_{3\to4}\Big(S_{2\to3}\Big(S_{1\to2}\big(\hat{\rho}(t_1^+)\big)\Big)\Big)\Big). \tag{11}$$

Because the compression and expansion strokes are unitary the system is isolated from the baths; i.e., no heat can be exchanged. In presence of vanishing heat the mean work output determines the average work via the sole difference of average energies of the system. This implies that the average work for the compression and expansion strokes are defined by the average of the two projectively measured energies of the isolated system [58, 67]; i.e.,

$$\langle W_{1\to2}\rangle = \langle E_2\rangle - \langle E_1\rangle\,, \tag{12}$$
$$\langle W_{3\to4}\rangle = \langle E_4\rangle - \langle E_3\rangle\,, \tag{13}$$

where the average energies are

$$\langle E_i\rangle = \mathrm{tr}\left(\hat{H}(t_i)\hat{\rho}(t_i)\right). \tag{14}$$

Clearly the average energy can also be computed using the post measurement density operator giving $\langle E_i\rangle = \mathrm{tr}\left(\hat{H}(t_i)\hat{\rho}(t_i^+)\right)$.

Keeping in mind that the baths are weakly coupled to the system, heat exchange with any bath is solely given by the negative of the corresponding bath energy changes. Moreover, during the strokes $2\to3$ and $4\to1$ the system Hamiltonian does not change; put differently, *no* work is applied on the *total* system composed of system and baths including the weak mutual interactions (energy conservation). Therefore, the average work applied to the system with the control parameter for $\hat{H}$ held constant is vanishing as well [32, 69]. The balance of energies exchanged thus implies that average heat exchange follows from a corresponding change in bare system energy alone, assuming here that the system Hamiltonian is not dressed by its interaction with the environment [71]. The average system energies are evaluated from the corresponding quantum state reached at the corresponding times $\{t_i\}$. These mean values follow from the set of projective measurements of the system Hamiltonian by use of the corresponding reduced density operator for the system at time $\hat{\rho}(t_i)$.

Accordingly, we hence find that the average values of heat exchanged are determined by

$$\langle Q_{2\to3}\rangle = \langle E_3\rangle - \langle E_2\rangle\,, \tag{15}$$
$$\langle Q_{4\to1}\rangle = \langle E_1\rangle - \langle E_4\rangle\,. \tag{16}$$

The net work of the cycle is thus given by

$$\langle W\rangle = \langle W_{1\to2}\rangle + \langle W_{3\to4}\rangle \tag{17}$$

The efficiency of this cycle can be appropriately defined as the ratio involving the net average work output $\langle W\rangle$ divided by the net heat transferred from the hot bath into the system, $Q_{2\to3}$. Note that here we adopt a negative sign convention for the net work, because we are primarily interested in a thermodynamic engine which does work on a load. The efficiency η for this quantum Otto cycle is thus given by

$$\eta = -\frac{\langle W\rangle}{\langle Q_{2\to3}\rangle}\,. \tag{18}$$

III. OPTIMAL TIME DISTRIBUTION BETWEEN UNITARY STROKES

Next, we numerically investigate different scenarios in which the operations are performed in finite-time. For details of our numerical analysis, we refer the readers to Appendix A. We begin by first considering the cases in which the time spans of the processes $2\to3$ and $4\to1$ (i.e. $r_b\tau_b$ and $(1-r_b)\tau_b$) are both sufficiently long, such that we can safely assume that the quantum states 1 and 3, after the respective dissipative strokes, are given by a thermal-like quantum state; i.e.,

$$\hat{\rho}_i = \sum_n \frac{e^{-(n+1/2)\beta_i\hbar\omega_i}}{Z(\beta_i,\omega_j)}|n\rangle\langle n| \tag{19}$$

where $i=1,3$, $\omega_3=\omega_2$. Upon combining Eqs. (7), (9) and (12-14), it is possible to compute $\langle W_{1\to2}\rangle$ and $\langle W_{3\to4}\rangle$. Note [74, 75] for analytical expressions of the mean work for various forms of $\omega(t)$.

We next search for the optimal distribution of the total time spent on the unitary processes τ_u between the two strokes, which is parametrized by r_u. For instance, for

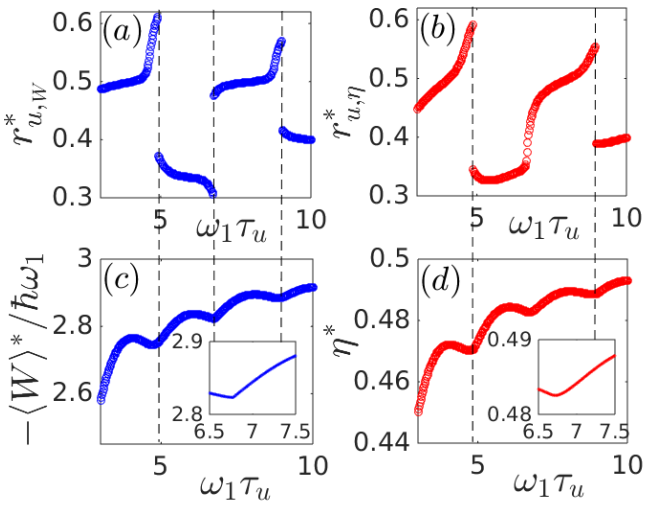

FIG. 2. (color online) **Optimal distribution of times between strokes.** Optimal values of the unitary parameter (a) $r^*_{u,W}$ and (b) $r^*_{u,\eta}$ that optimize respectively, the work extracted $\langle W\rangle/\hbar\omega_1$ and efficiency η versus τ_u. (c) The optimal work, $\langle W\rangle^*$, corresponding to the values of $r^*_{u,W}$ in (a) as a function of τ_u. (d) Maximal efficiency η^* corresponding to the values of $r^*_{u,b}$ in (b) a function of τ_u. Hamiltonian and bath parameters are $\omega_2 = 2\omega_1, \beta_1\hbar\omega_1 = 0.5, \beta_3\hbar\omega_1 = 0.1$ for all cycles. The insets in (c,d) are close-ups of the respective quantities at $\omega_1\tau_u \approx 6.8$, where $r^*_{u,W}$ changes discontinuously while $r^*_{u,\eta}$ changes smoothly. We note that the derivative of the optimal work $\langle W\rangle^*$ changes abruptly while that of the maximum efficiency η^* is smooth. The vertical dashed black lines indicate the position of the jumps of $r^*_{u,W}$ and $r^*_{u,\eta}$.

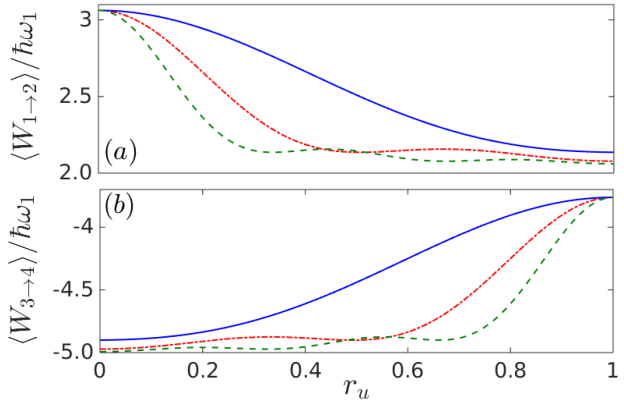

FIG. 3. (color online) **Work transfer of a single compression and expansion process.** (a) $\langle W_{1\to2}\rangle/\hbar\omega_1$ and (b) $\langle W_{3\to4}\rangle/\hbar\omega_1$ as a function of r_u for the compression arm of an Otto cycle that operates between ω_1 and $\omega_2 = 2\omega_1$ with $\tau_u\omega_1 = 2$ (continuous blue line), $\tau_u\omega_1 = 4$ (dash-dotted red), $\tau_u\omega_1 = 6$ (dashed green). Inverse temperatures of the bath are held at $\beta_1\hbar\omega_1 = 0.5$ and $\beta_3\hbar\omega_1 = 0.1$ respectively for the compression and for the expansion processes.

$r_u = 0$ the stroke from $1 \to 2$ constitutes an abrupt quench while a total of time τ_u is spent in the stroke $3 \to 4$. For larger values of r_u the time spent in the stroke from $1 \to 2$ increases while the one from $3 \to 4$ decreases until $r_u = 1$, i.e., when this last stroke becomes an abrupt quench. The ratio r_u for which the net work is optimum is referred to as $r^*_{u,W}$ and we denote the maximum work as $\langle W\rangle^*$, given by

$$-\langle W\rangle^* = \max_{r_u}\left(-\langle W\rangle\right) \tag{20}$$

(we remind the reader that the net work for an engine is negative). We depict with Fig. 2(a) the value of $r^*_{u,W}$ as a function of the total time spent on the unitary strokes τ_u. We observe that at some critical values of τ_u, discontinuities in the ratio $r^*_{u,W}$ occur. At the occurrence of these jumps, also the derivative of the net work output changes abruptly, see Fig. 2(c) and its inset.

A similar result emerges when r_u is chosen so as to maximize the efficiency, denoted here as $r^*_{u,\eta}$, see Fig. 2(b). The corresponding optimal efficiency is denoted as η^* and it is

$$\eta^* = \max_{r_u}\left(\eta\right). \tag{21}$$

The maximum efficiency η^* as a function of τ_u is shown in Fig. 2(d). In Fig. 2(b) we observe that the abrupt jumps are also present in the values of $r^*_{u,\eta}$, although they occur at different values of τ_u from the jumps in $r^*_{u,W}$. Moreover, in certain regions of τ_u an abrupt jump of $r^*_{u,W}$ can occur while a continuous variation of $r^*_{u,\eta}$ occurs, as is the case for $\omega_1\tau_u \approx 6.8$, see the insets of Fig. 2(c,d). Hence, given a total time τ_u for the unitary strokes, the optimal distribution of times between the strokes $1 \to 2$, e.g. $r_u\tau_u$, and $3 \to 4$, e.g. $(1 - r_u)\tau_u$, depends on the quantity being optimized for; For instance either the net output work or the efficiency. Also note that values of our numerically evaluated optimal efficiency are always below that of the Carnot bound $\eta_C = 1 - \frac{\beta_3}{\beta_1} = 0.8$ as they should be.

The nonlinear behavior in the optimal ratio $r^*_{u,W}$ and $r^*_{u,\eta}$ can be understood by analyzing the work output from a single compression $\langle W_{1\to2}\rangle$, or expansion process $\langle W_{3\to4}\rangle$. As can be seen from Fig. 3 (see also [18]), the work transferred in a single unitary stroke becomes a non monotonic function of the ratio r_u when the value of τ_u becomes sufficiently large. This behavior is ultimately responsible for the phenomenon we observe. In fact, finding the optimal time spans between the strokes stems from matching the optimal work output from two non-monotonic functions of time under the constraint of a given total time spent on the two unitary strokes. In Fig. 3 we observe that the number of oscillations present in the work output as a function of r_u increases with the duration of total time spent on the two unitaries τ_u

In Fig. 4, the value of average work (left) and efficiency (right) as a function of the ratio r_u are shown for different values of τ_u. Since the work in each stroke is a

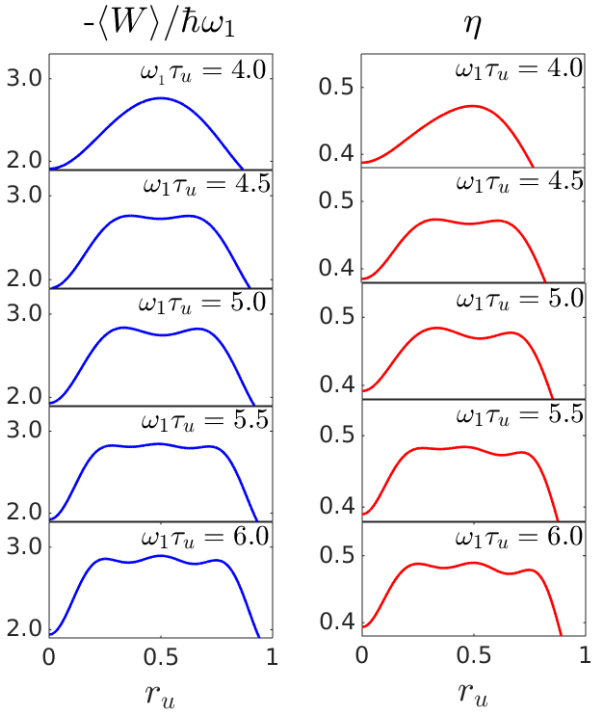

FIG. 4. (color online) **Oscillations of the net work and efficiency.** (Left panels) Mean work extracted and (Right panels) efficiency of cycles as a function of r_u for cycles with the parameters set at $\omega_2 = 2\omega_1, \beta_1\hbar\omega_1 = 0.5, \beta_3\hbar\omega_1 = 0.1$. Increasing number of oscillations in both net work and efficiency with the unitary timescale τ_u results in discontinuities in $r^*_{u,W}$ and $r^*_{u,\eta}$.

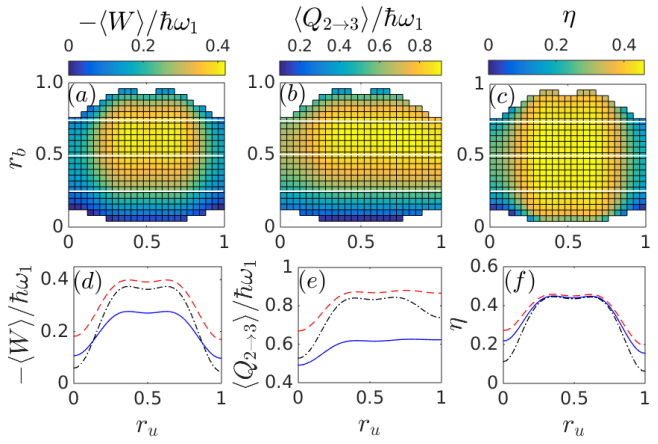

FIG. 5. (color online) **Cycle Performance at short bath coupling timescales.** (a) Average net work $\langle W\rangle$, (b) average heat from the hot bath $\langle Q_{2\to3}\rangle$ and (c) efficiency η of Otto cycles where $\omega_1\tau_u = \omega_1\tau_b/10 = 5$ as a function of r_u and r_b. Regions that are shaded white are domains in which the cycle is non physical as it is not doing work but instead receiving it. Plot (d-f) show the horizontal cuts highlighted by white lines in figures (a-c). In particular, in (d-f) the blue continuous line corresponds to $r_b = 0.25$, the red dashed line to $r_b = 0.5$, and the black dot-dashed line to $r_b = 0.75$. We use $\lambda^-_{1,3} = \omega_1/10$, $\lambda^+_3 = \lambda^-_3/e$ and $\lambda^+_1 = \lambda^-_1/e^{10}$ which corresponds to $\beta_1\hbar\omega_1 = 10$ and $\beta_3\hbar\omega_1 = 0.5$.

non-monotonic function of the time spent, the net work, which is the sum of work in the two unitary strokes becomes an oscillating function. For larger τ_u-values the number of local minima or maxima of the net work output, or of the efficiency, increases as the total time in the unitary strokes increases. The emergence of a new global extremum can occur either via the increase in magnitude of a local extremum, such that it becomes the global one, or when the global extremum turns unstable and in turn yields two extrema, with one of the two becoming the new global extremum. The former route is reminiscent of the behavior of the free energy as a function of the order parameter as temperature changes in an ordinary first order phase transition, while the latter mimics the behavior of a second order phase transition.

IV. OPTIMAL TIME DISTRIBUTION WITHIN UNITARY AND DISSIPATIVE STROKES

In the previous section, the state at the beginning of the compression and expansion strokes, 1 and 3 respectively, were assumed to be effectively thermal-like (because enough operation time was spent on the two dissipative strokes $2 \to 3$ and $4 \to 1$). We now consider the case in which the time spans of the dissipative strokes, $r_b\tau_b$ and $(1-r_b)\tau_b$, are too short for thermalization to occur such that the quantum states in 1 and 3 are no longer thermal-like. Under such circumstances, as detailed with Eq. (11), $\hat{\rho}(t_i^+)$ is the (unique) fixed point of the four strokes which connects the quantum state 1 back to itself.

Since after each energy measurement the density operator is diagonal in the basis of instantaneous energy eigenstates, computing $\hat{\rho}(t_1^+)$ amounts to finding the eigenvector associated to the eigenvalue 1 of the corresponding Markovian map in Eq. (11). In particular, we would like to stress that the numerical evolution of Eq. (1) in the strokes $2 \to 3$ and $4 \to 1$ is particularly simple because after the measurements in 2 and 4 the density operator is diagonal in the instantaneous eigenbasis of $\hat{H}(t_i^+)$. Moreover, our specific choice of dissipator $\mathcal{D}$, given by Eq.(3), preserves the diagonal form when acting on a diagonal density operator. This implies that the density operator, in the strokes $2 \to 3$ and $4 \to 1$ commutes with the Hamiltonian and hence its evolution only depends on the part involving the dissipation.

In order to stay in the weak coupling regime throughout the evolution, we ensure that the ratio $\lambda_i^\pm/\omega_1$ is always much lesser than 1. However, given the stylized setup of our system, keeping the products $\lambda_3^\pm r_b\tau_b$ and $\lambda_1^\pm(1-r_b)\tau_b$ fixed while varying $\lambda_i^\pm$, r_b and τ_b individually, results in the same $\hat{\rho}(t_i^+)$ obtained and hence leads to the same net work output and efficiency for the cycle [76].

In Fig. 5 we depict the color coded intensity for net average work $\langle W\rangle$, average heat input $\langle Q_{2\to3}\rangle$ and the efficiency η [cf. in Fig. 5, panels (a), (b) and (c)]. We choose $\tau_u = \tau_b/10 = 5/\omega_1$ because this is a long enough time to obtain two extrema in the cycle work output when the total time is distributed across the strokes (there would be only one maximum for shorter timescales). It should also be noted that in Fig. 5 some regions are colored in white. These regions correspond to cases (similarly to [52–54]) for which the finite-time operation of the cycle does not yield an overall negative net work output. Notably, these regions occur when any one of the dissipative or unitary strokes is performed in too short a time. In Fig. 5 we observe a quantitative change of the mean work output, heat and efficiency due to the finite time spent on the dissipative strokes, but do not find any qualitative changes. This is highlighted in Fig. 5(d-f) by the horizontal cuts of the intensity maps in Fig. 5(a-c) for three different values of r_b.

V. CONCLUSIONS

With this work we investigated the efficiency, net work output and input heat for a quantum Otto engine operated in a finite time. The cycle we consider is composed of two unitary strokes connected by two dissipative strokes. During the total time $\tau = \tau_u + \tau_b$ of the cycle operation, a typically asymmetric portion is spent on the two unitary strokes of total duration τ_u and the remaining time span τ_b on the two dissipative strokes. We numerically evaluated the optimal distribution of time spans within the unitary and dissipative strokes while optimizing either the net work output or the efficiency. The distribution of times is parametrized by r_u and r_b such that the time in the stroke $1\to2$ is $r_u\tau_u$ and $2\to3$ is $r_b\tau_b$. In Sec. III we elaborated on the case in which the time spent in the dissipative strokes is long enough such that the baths effectively thermalize the system at the end of the stroke.

We observed that optimizing for the work output results in discontinuous jumps in r_u^* across values of τ_u. Likewise, optimizing for the efficiency results in a similar jump behavior, albeit in a different location along τ_u. This feature stems from a non-monotonic dependence of work output on the time spent in each unitary stroke. This phenomenon is present as well when the baths do not fully thermalize the system as shown in Sec. IV.

We would like to note that the engine cycle considered includes energy measurements at the end of each stroke. Because in quantum mechanics each measurement affects the system via a back action, and since energy measurements are necessary to obtain the net energy balance for work output and heat exchange, it is essential to detail these measurements after each individual stroke of the cycle. We also stress that in any of these strokes we encounter non-equilibrium scenarios as the energy balance is *not* between corresponding thermal equilibrium states. Put differently, all our energy balance relations are manifestly non-equilibrium relations that cannot be labelled 'thermodynamic first law' relations. The latter involves knowing the difference between two internal energy state functions.

In contrast to the the quasi-static and reversible Otto cycle in thermal equilibrium such features of abrupt jumps are absent. Therefore, it would be of interest to see if the features as depicted in our set of figures, are indeed present in an experiment of a quantum Otto cycle.

The study of finite-time quantum engine cycles is necessary for the implementation of such systems. As exemplified by this work, the dynamics involved in finite time quantum engine cycles is rich and should be studied thoroughly.

Acknowledgments D.P. acknowledges support from Singapore MOE Academic Research Fund Tier-2 project (Project No. MOE2014-T2-2-119, with WBS No. R-144-000-350-112) and fundings from SUTD-MIT IDC (Project No. IDG21500104). Y.Z. is supported by NTU SUG M4081346. D.P. also acknowledges fruitful discussions with F. Binder, S. Fazio, J. Goold, K. Modi, S. Vinjanampathy.

Appendix A: Numerical computations

After each stroke, inclusive of the energy measurement, the density operator $\hat\rho$ is diagonal in the instantaneous energy eigenbasis and can thus be written as

$$\hat\rho(t_i^+) = \sum_n \rho_n^D(t_i^+)\Pi_n(t). \tag{A.1}$$

where ρ_n^D is the n-th element of the diagonal density operator. For a unitary stroke from t_i^+ to t_{i+1}^+ we get, using Eq.(7) or (9)

$$\rho_n^D(t_{i+1}^+) = \sum_m P_{t_i,t_{i+1}}^{n,m}\ \rho_m^D(t_i^+) \tag{A.2}$$

where

$$P_{t_i,t_{i+1}}^{n,m} = |\langle n(t_{i+1})|\hat U_{t_i,t_{i+1}}|m(t_i)\rangle|^2. \tag{A.3}$$

The dissipative evolution for $t\in[t_i^+,\ t_k^+)$, due to Eqs.(1-3) is instead given simply by

$$\begin{aligned}\frac{d\rho_n^D(t)}{dt} = 2\big\{&n\lambda_k^+\rho_{n-1}^D(t) + (n+1)\lambda_k^-\rho_{n+1}^D(t)\\ &-\left[(n+1)\lambda_k^+ + n\lambda_k^-\right]\rho_n^D(t)\big\}\end{aligned} \tag{A.4}$$

where $i=2$ or 4 and $k=[(i+1)\mod(4)]$. This simple form of time evolution is due to the fact that the density operator $\hat\rho$ is diagonal in the instantaneous energy eigenbasis at all instances of the dissipative strokes and hence it commutes with $\hat H$. In our implementation we have kept $n=50$ eigenstates of the harmonic oscillator, which is sufficient for the effective temperatures and dynamics involved.

In our numerical simulations, we have rewritten Eq. (1-3) in terms of dimensionless parameters. Explicitly, by dividing Eq. (1) by ω_1, we obtain

$$\frac{d\hat{\rho}}{d\tilde{t}} = -\mathrm{i}\left[\tilde{H}(\tilde{t}), \hat{\rho}\right] + \tilde{\mathcal{D}}(\hat{\rho}, \tilde{t}) \ . \tag{A.5}$$

where $\tilde{t} = \omega_1 t$,

$$\tilde{H} = \hat{H}/\hbar\omega_1 = (\hat{n} + 1/2)\tilde{\omega}, \tag{A.6}$$

and

$$\mathcal{D}(\hat{\rho}, \tilde{t}) = \tilde{\lambda}^{+}(\tilde{t})\left(2\hat{a}^{\dagger}\hat{\rho}\hat{a} - \left\{\hat{a}\hat{a}^{\dagger}, \hat{\rho}\right\}\right) + \tilde{\lambda}^{-}(\tilde{t})\left(2\hat{a}\hat{\rho}\hat{a}^{\dagger} - \left\{\hat{a}^{\dagger}\hat{a}, \hat{\rho}\right\}\right) \ ,$$

where $\tilde{\omega} = \omega/\omega_1$ and $\tilde{\lambda}^{\pm} = \lambda^{\pm}/\omega_1$. As a consequence the inverse temperature β can be written in dimensionless form $\tilde{\beta} = \beta\hbar\omega_1$ because

$$\beta\hbar\omega = (\beta\hbar\omega_1)\,(\omega/\omega_1) = \tilde{\beta}\tilde{\omega}. \tag{A.7}$$

[1] J. Gemmer, M. Michel, and G. Mahler, *Quantum Thermodynamics: Emergence of Thermodynamic Behavior Within Composite Quantum Systems*, 2-nd ed., Lect. Notes Phys. **784**, 1-346 (Springer, Berlin, 2009).
[2] P. Hänggi and F. Marchesoni, Rev. Mod. Phys. **81**, 387 (2009).
[3] K. Sekimoto, *Stochastic Energetics*, Lect. Notes Phys. **799**, 1-322 (Springer, Berlin, 2010).
[4] D. Gelbwaser-Klimovsky, W. Niedenzu, and G. Kurizki, *Adv. in atomic, molecular and optical physics* **64**, 329 (2015).
[5] J.P. Pekola, Nature Physics **11**, 118 (2015).
[6] P.G. Steeneken, K. Le Phan, M.J. Goossens, G.E. J. Koops, G.J.A.M. Brom, C. van der Avoort, and J.T.M. van Beek, Nature Physics **7**, 354 (2011).
[7] V. Blicke C. Bechinger, Nature Physics **8**, 143 (2012).
[8] J. Roßnagel, S. Dawkins, K. Tolazzi, O. Abah, E. Lutz, F. Schmidt-Kaler, and K. Singer, arxiv:1510.03681 (2015).
[9] M. Demirplack and S.A. Rice, J. Chem. Phys. **129**, 154111 (2008).
[10] M.V. Berry, J. Phys. A: Math. Gen. **42** 365303 (2009)
[11] J.W. Deng, Q.-H. Wang, Z.H. Liu, P. Hänggi, and J. B. Gong, Phys. Rev. E **88**, 062122 (2013).
[12] M. Palmero, E. Torrontegui, D. Guéry-Odelin, and J. G. Muga, Phys. Rev. A **88** 053423 (2013).
[13] E. Torrontegui, S. Ibáñez, S. Martínez-Garaot, M. Modugno, A. del Campo, D. Guéry-Odelin, A. Ruschhaupt, X. Chen, and J. G. Muga, Adv. At. Mol. Opt. Phys. **62**, 117 (2013).
[14] C. Jarzynski, Phys. Rev. A **88**, 040101 (2013).
[15] S. Deffner, C. Jarzynski, and A. del Campo, Phys. Rev. X **4**, 021013 (2014).
[16] A. del Campo, J. Goold, and M. Paternostro, Sci. Rep.**4**, 6208 (2014)
[17] A. del Campo, Phys. Rev. Lett. **111**, 100502 (2013)
[18] T.V. Acconcia, M.V.S. Bonança, and S. Deffner, Phys. Rev. E **92**, 042148 (2015).
[19] A. del Campo, M.M. Rams, and W.H. Zurek, Phys. Rev. Lett. **109**, 115703 (2012).
[20] S. Campbell, G. De Chiara, M. Paternostro, G. M. Palma, and R. Fazio, Phys. Rev. Lett. 114, 177206 (2015).
[21] W. Rohringer, D. Fischer, F. Steiner, I. E. Mazets, J. Schmiedmayer, and M. Trupke, Scientific Reports **5**, 9820 (2015).
[22] Y. Zheng, S. Campbell, G. De Chiara, and D. Poletti, arxiv:1509.01882 (2015).
[23] J. Yi, Y.W. Kim, and P. Talkner, Phys. Rev. E **85**, 051107 (2012).
[24] Z. Gong, S. Deffner, and H.T. Quan, Phys. Rev. E **90**, 062121 (2014).
[25] Y. Zheng and D. Poletti, Phys. Rev. E **92**, 012110 (2015).
[26] J. Jaramillo, M. Beau, and A. Del Campo, arxiv:1510.04633 (2015).
[27] R. Kosloff, Entropy **15**, 2100 (2013).
[28] R. Kosloff and A. Levy, Ann. Rev. Phys. Chem, **65**, 365 (2014).
[29] S. Vinjanampathy and J. Anders, arxiv:1508.06099 (2015).
[30] J. Goold, M. Huber, A. Riera, L. del Rio, and P. Skrzypczyk, arxiv:1505.07835 (2015).
[31] P. Hänggi and P. Talkner, Nature Physics **11** 108 (2015).
[32] M. Campisi, P. Hänggi, and P. Talkner, Rev. Mod. Phys. **83**, 771 (2011).
[33] M. Campisi, P. Hänggi, and P. Talkner, Rev. Mod. Phys. **83**, 1653 (2011).
[34] C. Jarzynski, Phys. Rev. Lett. **78**, 2690 (1997).
[35] G.E. Crooks, Phys. Rev. E **60**, 2721 (1999).
[36] F. Douarche, S. Ciliberto, A. Petrosyan, and I. Rabbiosi, Europhys. Lett. **70**, 593 (2005).
[37] T. B. Batalhao, A.M. Souza, L. Mazzola, R. Auccaise, R. S. Sarthour, I. S. Oliveira, J. Goold, G. De Chiara, M. Paternostro, and R.M. Serra, Phys. Rev. Lett. **113**, 140601 (2014).
[38] S. An, J. N. Zhang, M. Um, D. Lv, Y. Lu, J. Zhang, Z.Q. Yin, H.T. Quan, and K. Kim, Nature Physics **11**, 193 (2015).
[39] M. Campisi and R. Fazio, arxiv:1603.05024 (2016).
[40] M. Campisi and R. Fazio, arxiv:1603.05029 (2016).
[41] O. Abah, J. Roßnagel, G. Jacob, S. Deffner, F. Schmidt-Kaler, K. Singer, and E. Lutz, Phys. Rev. Lett., **109**, 203006 (2012).
[42] O. Abah and E. Lutz, EPL, **106**, 2, (2014).
[43] R. Alicki, and D. Gelbwaser-Klimovsky, New J. Phys. **17**, 115012 (2015).
[44] B. Leggio, M. Antezza, arxiv:1601.08137 (2016).
[45] P. Mehta and A. Polkovnikov, Ann. Phys. (N.Y.), **332**, 110 (2013).
[46] J.H. Jiang, B.K. Agarwalla, and D. Segal, Phys. Rev. Lett., **115**, 040601 (2015).
[47] Y. Rezek and R. Kosloff, New J. Phys. **8**, 83 (2006).
[48] T. Feldmann and R. Kosloff, Phys. Rev. E. **61**, 4774 (2000).
[49] E. Geva and R. Kosloff, J. Chem. Phys. **96**, 3054 (1992).

[50] T. R. Gingrich, G. M. Rotskoff, S. Vaikuntanathan, and P. Geissler, New J. Phys. **16**, 102003 (2014).

[51] P. S. Pal, A. Saha, and A.M. Jayannavar arxiv:1601.00854 (2016).

[52] T. Feldmann and R. Kosloff, Phys. Rev. E. **68**, 016101 (2003).

[53] T. Feldmann and R. Kosloff, Phys. Rev. E. **85**, 051114 (2012).

[54] T. Feldmann and R. Kosloff, arXiv:1508.06495 (2015).

[55] R. Uzdin and R. Kosloff, New J. Phys. **16**, 095003 (2014).

[56] T. Feldmann and R. Kosloff, Phys. Rev. E. **73**, 025107(R) (2006).

[57] A. Alecce, F. Galve, N. Lo Gullo, L. DellAnna, F. Plastina, and R. Zambrini, New J. Phys. **17**, 075007 (2015).

[58] P. Talkner, E. Lutz, and P. Hänggi, Phys. Rev. E **75**, 050102 (2007).

[59] H. T. Quan, Y.-X. Liu, C. P.Sun, and F. Nori, Phys. Rev. E **76**, 031105 (2007).

[60] Y. Zheng, and D. Poletti, Phys. Rev. E **90**, 012145 (2014).

[61] R. Alicki, J. Phys. A **12**, 5 (1979).

[62] D. Leibfried, R. Blatt, C. Monroe, and D. Wineland, Rev. Mod. Phys. **75**, 281 (2003).

[63] V. Gorini, A. Kossakowski, and E.C.G. Sudarshan, J. Math. Phys. **17**, 821 (1976).

[64] G. Lindblad, Comm. Math. Phys. **48**, 119 (1976).

[65] J.I. Cirac, R. Blatt, P. Zoller and W.D. Phillips, Phys. Rev. A **46**, 2668 (1992).

[66] P. Talkner, P. Hänggi, and M. Morillo, Phys. Rev. E **77**051131 (2008).

[67] P. Talkner and P. Hänggi, Phys. Rev. E **93**, 022131 (2016).

[68] G. Watanabe, B. P. Venkatesh, P. Talkner, M. Campisi, and P. Hänggi, Phys. Rev. **89**, 032114 (2014).

[69] P. Talkner, M. Campisi, and P. Hänggi, J. Stat. Mech.: Theor. Exp., **P02025**, (2009).

[70] For this to hold true the weak system-bath coupling assumption is most essential. Generally, a non-vanishing interaction will lead to a Hamiltonian operator of mean force $\hat{H}^*(t)$ [71–73]. Focussing on thermal equilibrium, this Hamiltonian operator of mean force $\hat{H}^*$ dresses the bare system Hamiltonian $\hat{H}$ in presence of non-vanishing system-bath interactions, making it generally dependent on both the inverse temperature β and also on the coupling strength(s). The internal energy change is then no longer given by a difference of the corresponding bare system Hamiltonians $\hat{H}(X(t))$, with $X(t)$ denoting a time-dependent control parameter. Instead the average internal energy of the system $E \to U$ becomes dressed, reading, $U = -\partial \ln Z/\partial\beta = \langle \hat{H}^* \rangle + \beta \langle \frac{\partial \hat{H}^*}{\partial \beta} \rangle$. Here, the angular brackets denote a trace over the reduced thermal equilibrium density operator for the system, which is given in terms of the Hamiltonian operator of mean force $\hat{H}^*$, with Z denoting its corresponding dressed partition function. In the present case of generally non-equilibrium quantum states and *weak* system-bath coupling we have that the system Hamiltonian $\hat{H}(X(t))$ does not become dressed. The averages of the system Hamiltonians $\hat{H}(X(t_i))$ are then averages taken over the corresponding time-dependent, reduced system density operator $\hat{\rho}(t_i)$.

[71] M. Campisi, P. Talkner and P. Hänggi, Phys. Rev. Lett. **102**, 210401 (2009).

[72] P. Hänggi, G.L. Ingold, and P. Talkner, New J. Phys. **10**, 115008 (2008).

[73] P. Hänggi and G.L. Ingold, Acta Phys. Pol. B **37**, 1537 (2006).

[74] S. Deffner and E. Lutz, Phys. Rev. E **77**, 021128 (2008).

[75] Y. Rezek, P. Salamon, K.H. Hoffmann, R. Kosloff, EPL, **85**, 30008 (2009).

[76] It should be stressed again that the master equation (1), and the computation of heat and work in the dissipative strokes, are valid only for small $\lambda_i^{\pm}$.